Relationships between intense convection, lightning, and rainfall over the interior Congo Basin using TRMM data

Stephen L. Solimine¹, Liming Zhou¹, Ajay Raghavendra², Yichen Cai^{1,3}

¹Department of Atmospheric and Environmental Sciences, University at Albany, Albany, New York, USA

²U.S. Army, Latham, New York, USA

³Atmospheric Sciences Research Center, University at Albany, Albany, New York, USA

Received 30 September 2021, Revised 28 February 2022, Accepted 25 March 2022, Available online 30 March 2022, Version of Record 1 April 2022.

Abstract

The lack of *in situ* observations across equatorial Africa creates forecasting challenges for regional populations affected by extreme weather events and makes accurate hydrological monitoring within the Congo Basin difficult. Due to the high mean convective intensity in this region, lightning observations may be particularly useful for improving satellite-based surface precipitation monitoring and forecasting. Therefore, this study aims to quantify the relative frequency of the most intense convective events in the Congo and their associated lightning precipitation relationships through the analysis of high-resolution Tropical Rainfall Measuring Mission (TRMM) radar and lightning observations for the years 1998 – 2013. Lightning and precipitation measurements associated with observed echoes were isolated and assigned to one of four categories of intense convective-stratiform echo types. Results show that only 2.7% of observed echoes were classified as intense convective-stratiform, yet they produced 36.6% of observed lightning flashes and 27.4% of estimated rain totals. Significant spatial correlations were also found between total rainfall and intense convective-stratiform rain (coefficient r = 0.56). Linear relationships between lightning and echo rain rates are shown to depend heavily on the convective category. As a result, a simple linear regression cannot be made for all intense convective echoes. However, lightning can be used to retrieve a lower-bound approximation with respect to convective rain rates. Results suggest that if properly implemented, the addition of lightning data may help to improve or constrain satellite derived convective intensity and rainfall estimations.

1 Introduction

The lack of a continuous *in situ* observation network across equatorial Africa makes it challenging to quantify the regional hydrological balance and its impacts on vegetation dynamics (Alsdorf et al., 2016; Zhou et al., 2014; Jiang et al., 2019). In addition, a dearth of surface radar observations makes short-range severe weather forecasting difficult for vulnerable socio-economic regions throughout the tropics. Therefore, the use of satellite retrievals is extremely important for surface precipitation monitoring and forecasting within these regions. Furthermore, the combination of high thunderstorm occurrence and strong mean convective intensity result in central Africa experiencing one of the greatest annual mean lightning flash rates in the world (Albrecht et al., 2011; Cecil et al., 2015). As a result, the addition of lightning observations to remote sensing rainfall estimations may be particularly useful across central Africa and the Congo Basin.

It has long since been established that colder cloud top temperatures (CTT) associated with deep convective clouds are generally linked to greater amounts of precipitation (Arkin, 1979; Negri and Adler, 1981), which has been the basis for many infrared (IR)-derived rainfall estimates (e.g., Adler and Negri, 1988; Arkin and Xie, 1994; Ebert and Manton, 1998; Kuligowski, 2002). This approach mainly involves the use of geostationary satellite observations which offer extensive areal coverage at relatively high spatiotemporal resolutions (4 x 4 km² every 30 minutes or less) and are available in many regions where surface and radar observations are mostly non-existent. Although these techniques can be used to fill observational gaps throughout the tropics, they have their own set of limitations. For instance, IR-derived rainfall may underestimate precipitation rates associated with newly forming convective systems due to their warmer CTTs. In addition, thick cirrus shields associated with mature mesoscale convective systems (MCSs) can obscure convective rain shafts resulting in an overestimation of precipitation (Adler and Negri, 1988; Vicente et al., 1998).

Improvements have been made through the combination of IR and visible (VIS) measurements (Kidd and Levizzani, 2011). The underlying theory is that very bright clouds tend to be associated with a much greater vertical cloud thickness which, when combined with very cold CTTs, can help to reduce errors associated with cold but relatively thin cirrus clouds. Geostationary visible retrievals also offer greater spatial resolution than IR and can resolve finer scale cloud features. Some of these techniques are still widely used today (Griffith et al., 1978; Arkin and Meisner, 1987; Adler and Negri, 1988; Ba and Gruber, 2001) but are only useful during daylight hours and may be affected by variations in solar zenith angle. More realistic precipitation retrievals can be made with both passive and active microwave sensors due to their ability to sense precipitation within deep convective clouds. Microwave sensors can also be used to improve results by calibrating IR-based techniques (Kidd et al., 2003; Kuligowski, 2002; Sorooshian et al., 2000; Todd et al., 2001); however, their exclusivity on low Earth orbiting (LEO) satellites results in poor sampling even when combining many available products (Hong et al. 2012).

The inclusion of lightning as an ancillary dataset, which can be utilized at any hour of the day, may improve forecasting accuracy related to high impact convective events due to its strong

connection to ice microphysics and convective intensity (Zipser, 1994; Petersen et al., 2005; Toracinta et al., 2002; Williams et al., 2002; Yuan et al., 2011). Gijben and de Coning, (2017) found a noticeable increase in nowcasting accuracy when incorporating lightning data into remote sensing algorithms designed to identify rapidly developing thunderstorms (RDT) in South Africa. Currently, however, only ground-based lightning detection networks provide the necessary temporal coverage for inclusion in short-range forecasting within the African continent. These networks have widely varying detection efficiencies and mainly detect cloud-to-ground (CG) lightning (Nag et al. 2015; Gijben, 2012), which account for only 25% and 30% of total lightning (intracloud (IC) + CG) flashes within the tropics and sub-tropics, respectively (Bandholnopparat et al., 2020). Additionally, RDTs in early development will produce mostly IC lightning, whereas CG lightning is more likely to occur with mature convective systems (Price, 2013). Therefore, it is imperative that any nowcasting systems utilizing lightning data have the capacity to efficiently detect both IC and CG lightning.

The Meteosat Third Generation (MTG) mission, scheduled for launch at the end of 2022, is a system of geostationary satellites with a Field-of-View (FOV) encompassing the entirety of the African continent. Among other instruments, these satellites will be equipped with a new Lightning Imager (LI) sensor capable of making continuous lightning measurements at storm scale resolutions (4.5 km at nadir) and will detect both IC and CG lightning (Holmlund et al., 2021). While there are no geostationary lightning measurements currently available over the African continent, studies elsewhere have demonstrated the utility of such datasets. Schultz et al., (2016) used measurements taken by the GOES-R Geostationary Lightning Mapper (GLM) to identify lightning jumps, rapid increases in lightning activity, as proxies for the automated tracking of storm systems in conjunction with radar measurements in the southern United States. In the meantime, however, LEO's capable of retrieving total lightning can be used to evaluate the relationship between lightning and deep convection over Africa in preparation for MTG operationality. The Tropical Rainfall Measuring Mission (TRMM) provides simultaneous total lightning and three-dimensional radar echo measurements associated with convective systems between 0° and $\pm 38^{\circ}$ latitude. Xu et al. (2013) demonstrated significant correlations between various lightning parameters and convective precipitation associated with storms over the southern United States by utilizing TRMM measurements. However, the dynamics and thermodynamics of intense convection varies between the mid-latitudes and deep tropics (Chaudhuri and Middey, 2014), which may result in regional differences in lightning-precipitation relationships. To the best knowledge of the authors, an extensive analysis related to variations in lightning-precipitation relationships in the Congo Basin as a function of convective development and diurnal cycle has yet to be conducted.

Through the analysis of 16 years of TRMM observations, the current study seeks to identify the storm-types responsible for the retrieved lightning and volumetric rain totals in the interior Congo Basin. Correlations between various lightning parameters and convective precipitation associated with each storm-type will then be presented along with diurnal variations in their respective relationship strengths. Therefore, the goals of this study are three-fold: to gain a deeper understanding of Congo Basin lightning activity and precipitation as it relates to intense convection, to identify key factors worth considering when interpreting general lightning-

precipitation correlations, and to evaluate the potential usefulness of lightning-based precipitation estimates when nowcasting for strong convection events.

2 Data and Methods

2.1 Study region

When defining the appropriate study region, it is important to consider any dominant local forcing mechanisms driving thunderstorm activity that may be non-representative of the area, namely the interior Congo Basin. In a study conducted by Raghavendra (2020), it was implied that yearly consistencies in the concentration, spatial orientation, and location of the African lightning maximum (Fig. 1), just west of the Rift Valley Mountain range, are the result of orographically induced deep convection. However, an analysis from Soula et al. (2016) of a much broader, secondary lightning maximum located within the Congo Basin lowlands indicated that the yearround wide spread convection was mainly driven by moist unstable air. Additionally, Laing et al. (2011) demonstrated the influence of sea-breezes on thunderstorm activity along the west coast of equatorial Africa, as well as its interactions with convective systems in the lee of the Cameroon mountains. To maintain regional consistency with respect to the development and behavior of thunderstorms examined in this study, coastal and orographically enhanced convective regions within and near the Congo Basin were excluded from analysis. The region of interest is, therefore, defined as the geographic area falling within 18°E-25°E longitude and 10°S-5°N latitude (black box in Fig. 1), and captures most of the peak lightning activity associated with moist convective processes within the interior Congo Basin. This region encompasses roughly 1.3 million km² of the Congo Basin.

2.2 Lightning data

Our lightning data comes from measurements taken by the Lightning Imager Sensor (LIS) onboard the TRMM satellite, provided by the NASA Global Hydrology Resource Center DAAC (http://dx.doi.org/10.5067/LIS/LIS/DATA201; Blakeslee, 2021), during the period 1998 - 2013. LIS detects lightning flashes at a resolution of 4 km over a 600 x 600 km² area. The staring sensor allows for each Earth location within its FOV to be continuously observed every 2 milliseconds for a period of 90 seconds. All lightning-flash data presented in this study has been scaled according to empirically derived detection efficiencies per local solar hour at the time of observation as provided by Cecil et al., (2014), which vary between ~ 70% at local noon and ~ 90% at night. Version 4 of the level 2 product was used to map retrieved flashes onto a lat-lon grid with a 0.05°, hourly spatiotemporal resolution for the years 1998 – 2013. In order to filter out observations where a temporary loss of data occurred, only pixels with an effective observation time of at least 80 seconds were used, similar to the approach in Cecil et al., (2015). Estimated flash rates are calculated by dividing the number of observed flashes per pixel by their effective observation time. A nominal orbital boost performed in 2001 resulted in slight changes to the LIS pixel resolution and imager FOV width, yet this was found to have no noticeable impact on lightning detection efficiencies (Cecil et al., 2014).

2.3 Precipitation and echo classification data

Precipitation and echo classification data were acquired from the University of Washington TRMM Database (UWTD) (http://trmm.atmos.washington.edu) supported by the NASA Earth Sciences PMM Program. The UWTD was derived from measurements made by the Precipitation Radar (PR) instrument onboard TRMM and archived at the Earth Sciences Data and Information Services Center (GES DISC). The PR instrument is an active microwave sensor capable of resolving the three-dimensional structure of precipitation. The whiskbroom scanner makes 49 cross-track observations over $\pm 17^{\circ}$, resulting in a swath width of 215 km and a horizontal pixel resolution of 5 km. It is important to point out that only TRMM-LIS lightning measurements that fall within the PR swath are used in this study. Portions of the database relevant to this study were compiled using the attenuation corrected reflectivity sub-product of TRMM-PR 2A25 (https://disc.gsfc.nasa.gov/datacollection/TRMM 2A25 7.html), and Rain Type classifications convective, stratiform, and other) designated by TRMM-PR as (https://disc.gsfc.nasa.gov/datacollection/TRMM 2A23 7.html); both are products of version 7 orbital data. The three-dimensional radar reflectivity retrievals from 2A25 were used to analyze the intensity and spatial extent of precipitating systems, referred to henceforth as "echo objects", "echoes" or "cores", for the period 1998 - 2013. Observed echo objects were geolocated and interpolated from radar coordinates onto a 3-D Cartesian grid with horizontal and vertical resolutions of 0.05° and 250 m (Houze et al., 2007, 2015). Echo objects in the interpolated dataset were separated into different categories based on rain type, intensity (dBZ), storm height, and horizontal area. The echo object classifications (echo-types) that we adopt from the UWTD for use in the present study are defined as follows:

- i. Detectable Rain Area (DRA): An echo object consisting of at least 2 contiguous pixels.
- ii. Deep Convective Core (DCC): Three-dimensional convective echo objects that exceed both intensity and height thresholds of 40 dBZ and 10 km.
- iii. Wide Convective Core (WCC): Three-dimensional convective echo objects that exceed both intensity and horizontal area thresholds of 40 dBZ and 1000 km².
- iv. *Deep-Wide Convective Core (DWC):* Three-dimensional convective echo objects that exceed both DCC and WCC thresholds.
- v. *Broad Stratiform Region (BSR):* Three-dimensional stratiform echo objects that exceed a horizontal area threshold of 50,000 km².

It should be noted that none of the echo objects in categories ii – v are a subset of one another (i.e., they are not counted twice), but all are considered a *strong* subset of the DRA category. The thresholds presented above have been empirically determined to encompass the most intense end of the convective-stratiform spectrum for land regions (Houze et al., 2015) and tend to represent the various stages of deep convective development (Zuluaga and Houze, 2013). Echo objects classified as DCCs are associated with young and vigorous convection, while DWCs and WCCs represent intense convective systems that have likely developed upscale into mature mesoscale convective systems. Broad Stratiform Regions (BSRs) are large convectively initiated stratiform

echoes associated with very well developed MCSs in later stages of development (Houze et al., 2015).

Statistics associated with echo objects belonging to each category are stored in tabular files and dimensioned by instance. Volumetric rain rate (kg s⁻¹), defined as the total mass of precipitation per unit time generated by the entire echo, and mean near surface rain rates (mm hr⁻¹) associated with individual echoes are included along with their date and time of occurrence, echo top height (km), horizontal area (km²), geographic centroid, and horizontal dimensions in the Cartesian plane. The tabular files were used to construct a gridded dataset for each category which consists of echo object bounding regions mapped onto a lat-lon grid with a 0.05°, hourly spatiotemporal resolution for the period 1998 – 2013. The echoes were analyzed using the provided parameters and compared with lightning data in order to compile lightning-flash and precipitation statistics for each category, and to determine lightning-precipitation relationships associated with echoes in the strong convective sub-classes (categories ii – iv). It is important to point out that all echoes belonging to categories ii – iv represent only the convective cores of larger cloud clusters or "storms". Therefore, it is implied that all precipitation statistics associated with each convective category do not include any associated stratiform components of rainfall.

2.4 Separating lightning by echo type

Lightning measurements are considered belonging to a specific echo type if they occur within any of their associated echo object bounding regions during the time of observation. Lightning flashes that fall within the overlapping regions of different strong convective categories are discarded due to classification uncertainty. However, since radar and lightning data are compared simultaneously, ambiguity with respect to flash-echo concurrence is exceedingly rare with < 1% of lightning observations meeting this criterion. Since BSRs generally form as the result of strong MCSs, they will at some point in their life cycle contain embedded convective cores (Houze et al., 2015). Flashes observed inside convective cores within BSR echoes are assigned to that convective category only. Therefore, flashes assigned to BSRs are those that occurred within their bounding regions but outside any embedded strong convective cores.

3 Results

3.1 Spatial distributions

The 16-year average of the number of observed strong convective-stratiform echoes and their associated volumetric rainfall totals are shown in Figures 2a – h. The black box in each figure represents the boundaries of the study region and values are plotted at a 1° x 1° horizontal resolution; the surrounding regions are included for context. In order to make direct comparisons between echo location points and rainfall, the displayed values are based on the location of echo centroids and are, therefore, not representative of the true spatial extent of associated rainfall. A concentrated peak in the number of convective echoes (i.e., DCCs, DWCs, and WCCs) can be seen just west of the Rift Valley Mountain range, which coincides with the lightning maximum in Figure 1. Similarly, a broader peak in the number of convective echoes is almost entirely enclosed by the bounds of the study region, particularly for DWCs and WCCs. These distributions coincide well with the secondary lightning maximum located over the interior Congo Basin as shown within

the black box of Figure 1. Between $10^{\circ}\text{S} - 5^{\circ}\text{N}$, BSRs tend to have a weak presence east of the eastern boundary of the study region, generally peaking within the interior Congo Basin. This is suggestive of the upscale development of convective systems into very well developed MCSs as they propagate westward from the peak occurrence region of the Rift Valley Mountain range.

Volumetric rainfall patterns associated with each category correlate well with their respective echo distributions, especially for DCCs and BSRs. The largest rainfall totals for DWCs and WCCs are further west of the concentrated peak in echoes near the Rift Valley Mountain range and occur well within the bounds of the study region. This is also likely due to the intensification of storms as they propagate westward. Figures 3a - h show the yearly mean percentage of DRA echoes and total volumetric rainfall associated with each strong category and are plotted at a 1° x 1° horizontal resolution. Except for DCCs, relatively large fractions of localized rainfall totals are produced from a relatively small fraction of observed echo objects within the study region. Indeed, a quantitative correlation analysis between yearly mean spatial volumetric rainfall totals and the sum of DWC, WCC, and BSR rainfall totals within each grid cell yield a correlation coefficient r of 0.56 (P < 0.01), which is significant when considering the small fraction of echoes associated with these events. These results qualitatively agree well with the spatial correlations between rainfall and MCSs studied in Jackson et al., (2009).

3.2 Regional statistics

A breakdown of echo object precipitation, occurrence, and lightning-flash count by category is expressed in Figures 4a – c as percentages of the total retrieved volumetric rain per unit time (kg s⁻¹), DRA echo occurrence, and lightning-flash count over the study region for the 16-year observation period. Although echoes classified as strong convective-stratiform only accounted for 2.7% of the total observed echo objects, they contributed 27% of the regional precipitation totals (Figs. 4a and b), emphasizing the significance of these storms in Congo Rainforest hydrology.

Of the lightning flashes observed by TRMM, 36.6% were associated with DCCs (6.3%), DWCs (10.3%), WCCs (17.9%) and BSRs (2.1%) (Fig. 4c). Figures 5a – c show the yearly mean frequency of echo occurrence (echoes yr⁻¹), echo lightning-flash count (fl echo⁻¹), and echo lightning-flash density (fl km⁻²) for categories ii – v. Echo lightning-flash count is defined as the average number of observed flashes within the bounding regions of each echo object (SUM[flashes year⁻¹]/SUM[echo objects year⁻¹]), and the echo lightning-flash density is defined as the yearly sum of observed echo flashes per unit echo area (SUM[flashes year⁻¹]/SUM[echo area year⁻¹]). The frequency of echo occurrence is merely the sum of all echo objects observed within the study region for each year (SUM[echo objects year⁻¹]).

Although lightning-flash density is nearly twice as high or greater in DCCs (i.e., young intense convection) than any other category (Fig. 5c), DWCs dominate with respect to the number of observed flashes per echo object (Fig. 5b). This can be explained by DWCs having a much greater core area than DCCs. The simultaneously high percentage of observed lightning flashes associated with WCCs (Fig. 4c), and their relatively low lightning-flash density and echo flash count (Figs. 5b and c) can be explained by their dominance in occurrence within the study region (Fig. 5a). Figure 5d shows the average echo top height and mean rain rate associated with

individual echo objects in each of the strong convective categories. The reduced lightning activity within WCCs coincides with much lower echo top heights in comparison to their deep convective counterpart. On the other hand, mean rain rates produced within WCCs are greatest despite their depressed echo top heights. On average, WCCs represent a more mature stage of mesoscale convective development when compared with DWCs (Zuluaga and Houze, 2013); therefore, while later stage MCSs exhibit similar or greater rainfall rates as those in earlier stages, they generate a significantly lower number of lightning flashes while still consisting of a large convective core region. Mean BSR echo flash frequency was slightly greater than that of WCCs (Fig. 5b); however, their lightning-flash density is much less than 1 flash per km², suggesting that the vast majority of BSR echo area does not contain lightning. It should be noted that BSRs are complex systems strongly associated with intense convection embedded within large stratiform regions (Houze et al., 2015), which helps explain the relatively comparable echo flash counts. Regardless, direct correlations between BSR lightning and precipitation are expected to be very weak or non-existent and will not be examined further.

3.3 Lightning-precipitation correlations

The relationship between echo object flash count and volumetric rain rate associated with individual cores of each strong convective category is visualized in Figure 6a. The correlation coefficient r for all strong convective echo objects combined is 0.36 (N = 2996). It is clear from the distribution of data points that a linear approximation in the relationship between lightning flash-count and volumetric rain rate is not appropriate for all convective categories and results in the relatively low correlation coefficient.

It is well known that the tallest deep convective clouds are associated with stronger updraft velocities and higher lightning flash rates. For instance, Yoshida et al., (2009) showed that flash rates within convective clouds were proportional to the fifth power of the cold-cloud depth. However, the highest flash rates are not necessarily associated with the most intensely precipitating echoes. Correlations between the mean echo pixel flash rates and echo volumetric rain rates for all strong convective categories revealed a weakly negative relationship (r = -0.23; P < 0.001; N = 2996). The mean echo pixel flash rates were calculated by taking the sum of all pixel flash rates and dividing by the number of lightning containing pixels within the echo (SUM[flash rate pixels]/SUM[# of lightning containing pixels]). In this study, echo flash counts are simply the sum of all measured flashes within a given echo object, which are strongly influenced by individual pixel flash rates. Therefore, the use of echo flash counts for rainfall estimates may not be ideal due to its inability to distinguish between smaller echoes with high flash rates and large, heavily precipitating echoes with a greater number of lightning containing pixels.

A more effective lightning parameter would be one that efficiently distinguishes between convective cores of various sizes, and thus, can more accurately estimate convective rain rates. Xu et al. (2013) found significant correlations between lightning-flash area and convective core area in storms over the continental United States (CONUS) (r = 0.75 - 0.85). While the dynamics related to thunderstorm formation in mid-latitudes varies from that in the tropics (Chaudhuri and Middey, 2014), the underlying ice-based microphysical processes driving storm electrification are assumed to be shared among all land regions (Yoshida et al., 2009).

Since it has been established that larger cores tend to produce greater amounts of rainfall (Atlas et al., 1990), and lightning observations per echo object have the potential to be greater within larger storms, lightning-flash area, defined here as the area of echo object grid cells containing at least one flash, may be a more useful proxy for estimating convective precipitation. Figure 6c exemplifies the very strong linear relationship between convective core area and volumetric rain rate (correlation coefficient r = 0.96) for all strong convective echoes. In addition, the relationship between echo object lightning-flash area and core area for all strong convective echoes is shown in Figure 6d. Although the correlation coefficient (r = 0.63; Fig. 6d) for echo objects over the study region is significantly lower than for convective cores analyzed over the CONUS by Xu et al., (2013), the combined results of Figures 6c and 6d suggest that volumetric rain rates should be well estimated by echo lightning-flash area. To assess this, the correlation analysis shown in Figure 6a was repeated, but with core lightning-flash area replacing flash counts (Fig. 6b). A notable increase in the correlation coefficient r by 0.20 confirms this assumption; however, a similar data distribution as seen in Figure 6a is evident, indicating that a simple linear relationship remains an unreasonable assumption.

It is clear from Figures 6a - b and d that the non-linear relationships mainly arise due to the inclusion of WCCs within the data distribution. Figures 7a - d show the same plots as Figures 6a - d but with all WCCs removed. Significant increases in correlation coefficients r by 0.33, 0.27, and 0.22 were calculated for Figures 7a, b, and d, respectively. The data distributions also exhibit a more linear relationship between the variables analyzed, particularly for Figures 7b and d.

3.3 Diurnal variations

Diurnal cycles of the normalized yearly mean echo frequency of occurrence, mean echo flash count, and mean echo volumetric rain for each echo type are shown in Figures 8a – d, and are displayed as percentages of their average daily sum. As suggested by Negri et al., (2002), a 4hour smoothing was applied to reduce errors introduced by the high spatial variability of TRMM sampling. Error bars represent the standard error about the mean (SE), where SE = $\frac{\sigma}{\sqrt{n}}$; σ and nare the standard deviation in echo parameters and the number of echoes observed within a given hour, respectively. For the mean echo frequency of occurrence, n is simply the number of years in the study. Although DCCs have a much sharper peak than DWCs, they are both most active in the mid-afternoon. However, evening activity in echo occurrence associated with DWCs is noticeably greater than for DCCs as their error bars do not overlap between 18z and 02z (Figs. 8a and b). A broad peak roughly stretching from 14z – 03z was found for WCCs, with the highest occurrence being around 00z (Fig. 8c). Activity associated with BSRs is greatest in the morning with a distinct peak occurring between 03z and 05z (Fig. 8d). All categories exhibit the highest amount of volumetric rain in the early morning hours, indicating that mainly heavier precipitating systems occur overnight. Both WCCs and BSRs are more likely to occur at late evening and overnight hours, which is in agreement with past studies (Zuluaga and Houze, 2015; 2013), and indicative of the upscale development of earlier occurring DCCs or DWCs into MCSs.

Unlike regional lightning-flash totals, which strongly reflect the number of observed thunderstorms, the hourly mean echo flash count measures the average amount of lightning produced within individual echoes at a given time of day. Echo flash counts associated with DCCs

exhibit a clear nocturnal peak in activity, particularly between 22z - 08z (Fig. 8a) and closely follow the diurnal cycle in volumetric rain rates. DWCs show a slight peak in echo lightning activity centered around 00z, but the overall trend remains relatively flat throughout the diurnal cycle (Fig. 8b). Both WCCs and BSRs show well defined echo flash count cycles with an average peak in the afternoon and low activity in the early morning, and are entirely out of phase with echo volumetric rain rates (Figs. 8c and d). The large error bars for all BSR parameters are the result of the low number of sampled echoes and high levels of variance among data points. Similarly, higher levels of uncertainty in the frequency of occurrence during peak hours for DCCs and DWCs are the result of high yearly variance in echo frequency at those times. It should be noted that there are very few observations of DCCs and DWCs during hours of minimum activity.

In order to explore any intra-categorical diurnal variations in lightning-precipitation relationships, results from a correlation analysis between lightning-flash area and volumetric rain rates among all strong convective morning echoes (01Z-10Z) were compared with afternoon and evening echoes (12Z-22Z). Results show a significant difference in correlations between morning and afternoon/evening echoes, with morning coefficients: r = 0.57 (P < 0.001; N = 353) and afternoon/evening coefficients: r = 0.74 (P < 0.001; N = 1006). Only 8 echoes were observed for both DCCs and DWCs during the designated morning hours, which is too few for a robust statistical analysis. However, an opposite pattern emerged when comparing nocturnal and diurnal WCC echoes alone: $r_{morning}$ [WCC] = 0.58 (P < 0.001; N = 337); $r_{evening}$ [WCC] = 0.45 (P < 0.001; N = 470).

4 Discussion

Although general correlations between lightning parameters and convective precipitation were found to be relatively poor to moderate, they do not fully capture the complexities of their relationship. High echo rain rates were found to occur at both high and low lightning-flash counts, while high flash counts are always associated with high echo rain rates. This causes the non-linear relationship observed between echo flash counts and convective volumetric rain rate. Nonetheless, this type of data distribution gives way to a lower bound in precipitation rate for a given amount of echo lightning-flash count. Therefore, minimum volumetric rainfall rates may be retrieved by incorporating lightning data into remote sensing rainfall estimations.

Lightning-flash area was found to be more closely correlated with convective rain rates, yet still exhibited a poor linear relationship. However, the ability of lightning-flash area to estimate convective core area (a strong proxy for volumetric rain rate) relatively well results in a much better defined and more well constrained lower bound in volumetric rainfall. The poorly defined upper boundaries in lightning-precipitation and lightning-core area relationships are mainly due to WCCs within the data distributions. This is evident when considering only strong deep convective echoes (i.e., DCCs and DWCs) in correlation analyses between lightning and precipitation where a strongly positive linear relationship emerges. In addition, once WCCs are removed, the correlation between echo lightning-flash area and core area agrees well with the results of Xu et al., (2013). Therefore, the prevalence of WCCs over the interior Congo Basin serves to weaken overall lightning-precipitation relationships compared to the intense convective events studied over the CONUS, and highlights their significance in tropical convection over land regions.

While the analysis of internal storm dynamics is beyond the scope of this paper, the retrieved echo top heights and diurnal cycles offer clues regarding the strength of convective updrafts and the dominant mesoscale forcings (e.g., low-level thermodynamic or elevated dynamic convection) associated with specific echo types. In addition, previous studies have described various dynamical characteristics of the echo types presented here (Rasmussen and Houze, 2011; Houze et al., 2015; Zuluaga and Houze, 2015, 2013). It is probable that differences in storm structure and dynamics can explain the disparities in results of the correlation analyses. For instance, DWCs represent a transitionary stage from intense discrete convection to large clusters of deep convective cells which may or may not have fully formed into an MCS at the time of observation. These large, extremely intense precipitation events have a relatively pronounced diurnal cycle with a late afternoon to early evening peak, suggesting that the convection associated with these storms likely originates from within the boundary layer and manifests as buoyancy driven plumes of rapidly rising air. The strong convective updraft regions within DWCs (as indicated by a high mean echo top height) are capable of producing significant amounts of lightning. Meanwhile, the overall large size of the convective aggregate results in the observed intensity in rainfall rates, and thus, a strong positive lightning-precipitation relationship. On the contrary, WCCs have a much lesser pronounced diurnal signal with a broad peak stretching from the afternoon into the early morning hours suggesting a weak direct dependence on diurnal heating and lower tropospheric buoyancy. Instead, these well-defined and mature MCSs have likely reached a stage in which local environmental adjustments occur in the form of a gravity wave response to the collective convective heating of the system (Houze, 2004). Under these circumstances, the system convection may become elevated with enhanced inflow shifted to the middle troposphere (Fovell, 2002). It is hypothesized that the lower storm top heights observed with WCCs are the result of weaker updraft velocities driven by the elevated heat source of the MCS in the absence of low-level thermodynamic forcing. Although these storms are more than capable of producing extreme rainfall rates, charging rates and the subsequent initiation of lightning would be significantly reduced by the weaker updrafts and much shallower cold cloud depths. Therefore, the lightning-precipitation relationship associated with this form of mature MCS is quite poor. Further in-depth analysis should be conducted in order to confirm this.

It has been demonstrated through previous studies that there exists a strong connection between updraft intensity and overall lightning production. Deierling and Petersen, (2008) showed that updraft volumes with a vertical velocity greater than 5 m s⁻¹ located above the -5°C isotherm were strongly correlated with total lightning activity (r = 0.93). Several other studies have also revealed that flash rates tend to be much higher and consist of smaller flashes in and near a strong updraft region, with an opposite tendency for flashes occurring further away from strong updrafts (Bruning and Macgorman, 2013; Carey et al., 2005; Kuhlman et al., 2009; Weiss et al., 2012). Therefore, it is reasonable to assume that DCCs consist mainly of large updraft regions with the greatest mean vertical velocities as they were found to have the highest mean lightning-flash density and pixel flash rates (not shown). The weakly negative correlation between mean echo flash rates and volumetric rain rates can be explained by the highest flash rates being a signature of very young, yet vigorous convection at a stage prior to maximum rainfall production. This stage of deep convection is best represented by DCCs that, in general, have lower rain rates.

In addition to variations in storm behavior among echo classifications, a distinct difference was noted between daytime and nighttime echoes. Despite WCCs experiencing relatively greater mean storm electrification during the afternoon, they showed a noticeable increase in lightning-precipitation relationship strength during the morning hours. Greater mean volumetric rain rates in the morning hours indicate that this is when the most intense convective echoes occur; these storms tend of have better defined lightning-precipitation relationships as was demonstrated by Figure 6b. The stronger lightning-precipitation relationships associated with all afternoon and evening convective echoes is likely due to the higher proportion of DWCs and DCCs at these times, which were shown to a have strongly positive lightning-precipitation relationship.

5 Study Limitations

The datasets used in this study present some limitations worth considering. For one, TRMM retrievals only show a brief snapshot of events, making the use of this data impossible for studying the evolution of individual storms through time. Therefore, the presented figures describe only a relative estimate regarding the ratio of precipitation and lightning totals assigned to each echo class, which could vary depending on the length of individual storm lifetimes. Furthermore, it has been suggested here that a weakly negative correlation between mean echo flash rates and volumetric rainfall may be the result of a potential lag between peak rain rates and lightning activity. If so, this would make it difficult to verify the true extent of their relationship when comparing simultaneously occurring measurements. For instance, it's possible that an increase in lightning-flash rates and total lightning activity within convective cores may be a precursor to greater upscale development and increased precipitation. On the other hand, the lightning detection efficiency of TRMM-LIS has been shown to be poor for flashes occurring within the lower altitude regions of deep convective clouds due to high optical depths (Thomas et al. 2000, Ushio et al. 2002). Therefore, it is possible that some lightning flashes within the most vertically thick DCCs and DWCs are not detected by TRMM, especially if they consist of smaller flashes generated by very large updraft velocities. This may result in some degree of correlation inaccuracy.

6 Summary and conclusions

This study utilized 16 years of high resolution TRMM data to examine the relationship between intense convection, lightning, and rainfall over the interior Congo Basin through the analysis of four well-known strong echo-types: DCC, DWC, WCC, and BSR, which tend to represent early, mature, late, and end-stage strong convection. Spatial analyses of the select convective-stratiform echoes revealed a strong spatial correlation between total rainfall and rainfall associated with DWCs, WCCs, and BSRs (i.e., MCS activity). A regional analysis of echo statistics emphasizes the significance of strong convective systems in Congo Basin hydrology and identifies the major mesoscale echo types associated with Africa's second most active lightning region. The combination of high retrieved rainfall ratios attributed to strong convective events, in conjunction with their contributions to regional lightning-flash totals, suggests lightning could serve as a potential proxy for aiding in the estimation and tracking of strong convective storms and rainfall throughout the Congo. The most prominent echo-type observed over the interior Congo Basin (WCCs) was shown to exhibit the weakest lightning-precipitation correlation. As a result, a simple linear regression is not a reasonable approach to rainfall estimations from lightning observations

within this region. However, a well-defined lower bound volumetric rain rate approximation can be calculated from lightning-flash area observations. The time of day may also affect the accuracy of lightning based volumetric rain rate estimations, which may be linked to diurnal variations in the dominant forcing mechanisms driving thunderstorm formation and the relative ratio of echo types. Storms which occurred in the afternoon and evening hours exhibited much stronger positive lightning-precipitation correlations than those occurring in the early morning. However, this is likely due to a greater number of deep convective storms occurring during the day. Morning storms among individual echo types tend to be stronger which results in echo populations that have stronger lightning-precipitation relationships, as was demonstrated with WCCs. Additionally, results suggest a potential lag between peak echo lightning activity and the time of maximum echo rainfall; however, this would require further analysis as the datasets used in this study contain only instantaneous information which does not allow for the analysis of individual storm evolution. Nonetheless, the incorporation of total lightning data into existing nowcasting techniques may assist in the determination of crucial unknowns (e.g., convective core area, stage of convective development, and updraft strength), which has the potential for improving their results if properly implemented.

Acknowledgments

This work is supported by the National Science Foundation (NSF AGS-1535426 and AGS-1854486). The authors would also like to thank the three anonymous reviewers for thoroughly reviewing the manuscript and offering valuable suggestions for improvement.

Figures

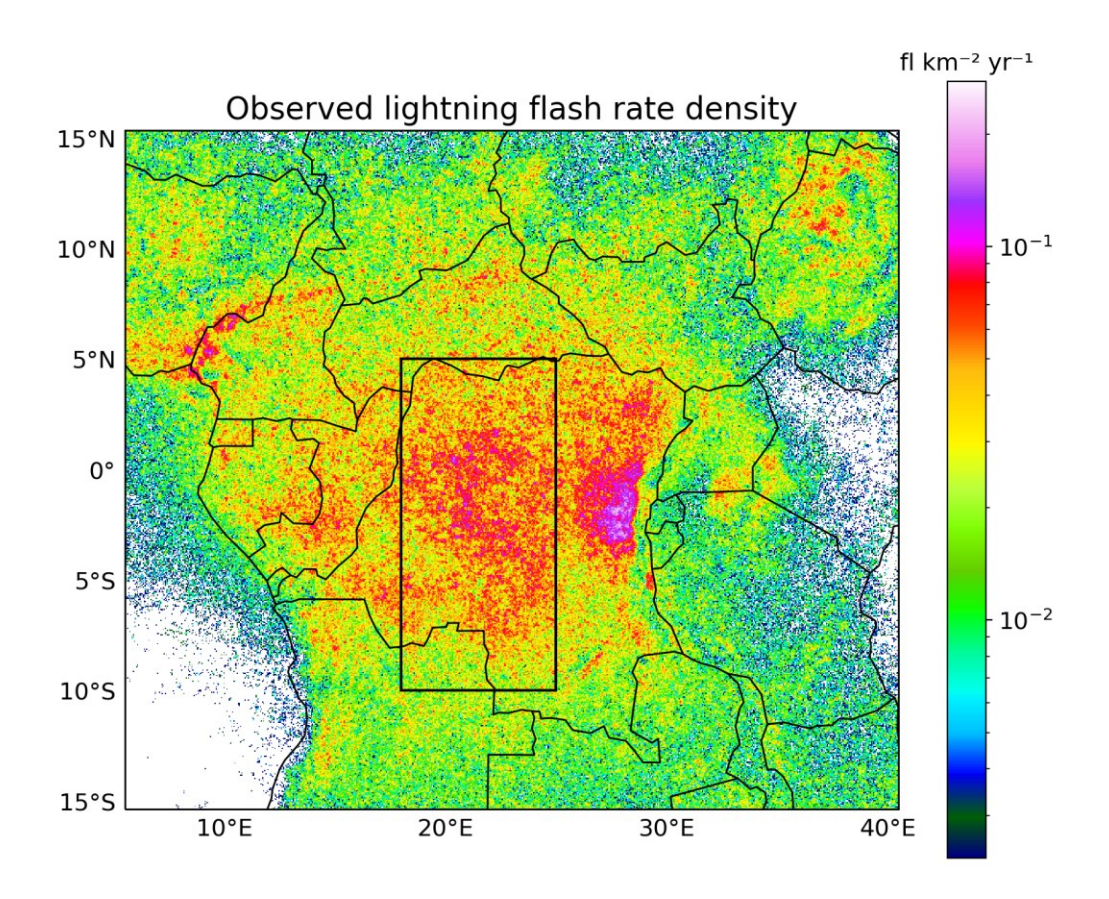


Figure 1: Lightning-flash rate density (fl km⁻² yr⁻¹) as directly observed by TRMM and calculated at a horizontal resolution of 0.05° . The black box represents the bounds of the study region.

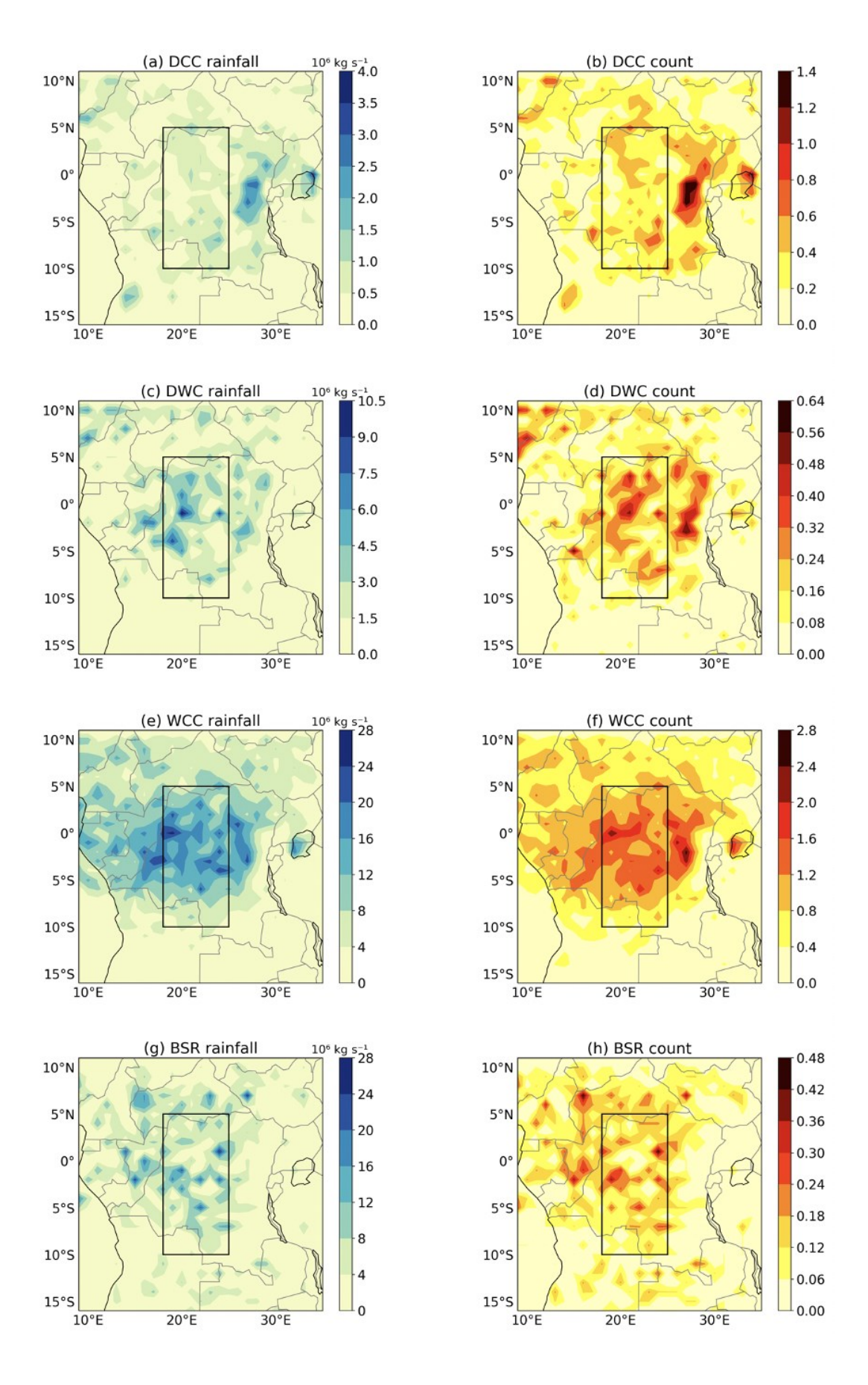


Figure 2: The yearly mean of volumetric rain rates ($10^6~kg~s^{-1}$) (left column) and number of observed echoes (right column) for each strong convective-stratiform category. Values are calculated at a $1.0\,^{\circ}$ horizontal resolution. The black box in each figure represents the bounds of the study region.

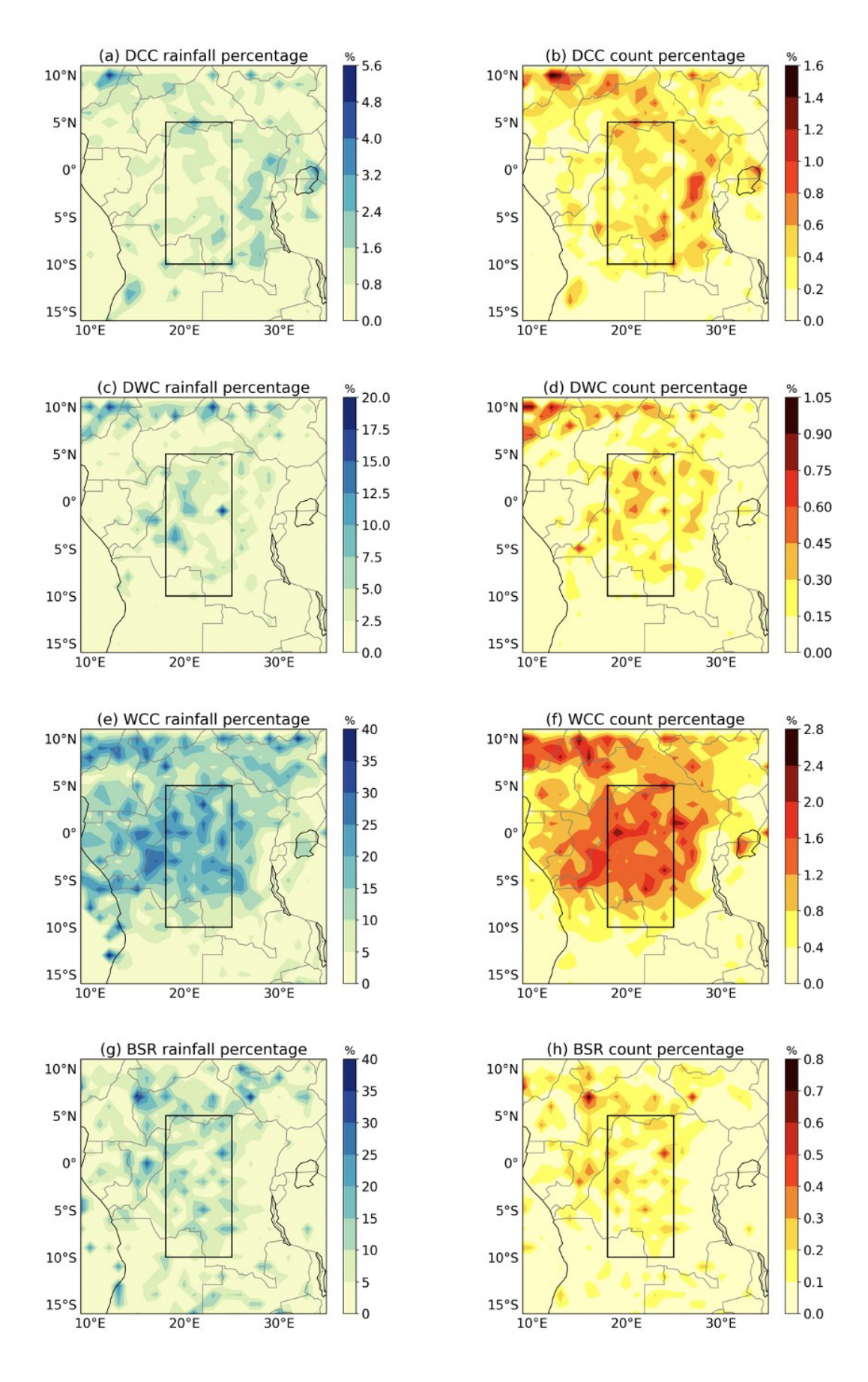
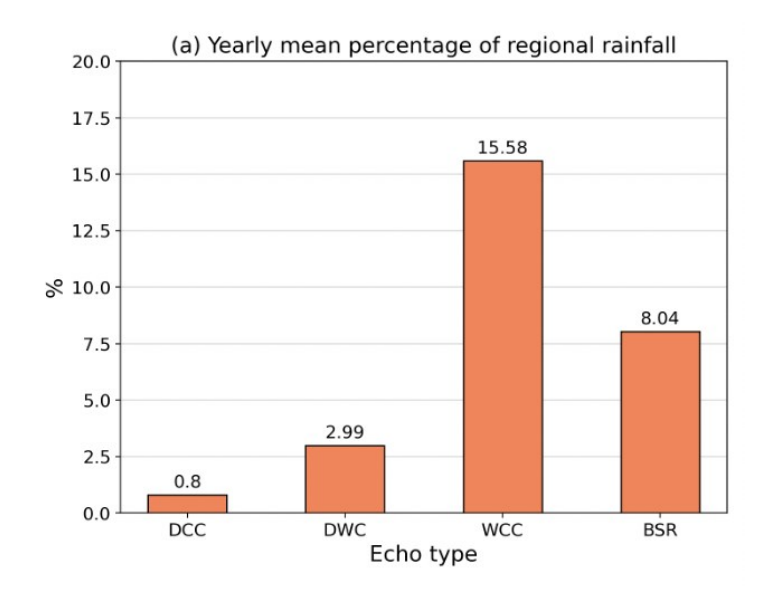
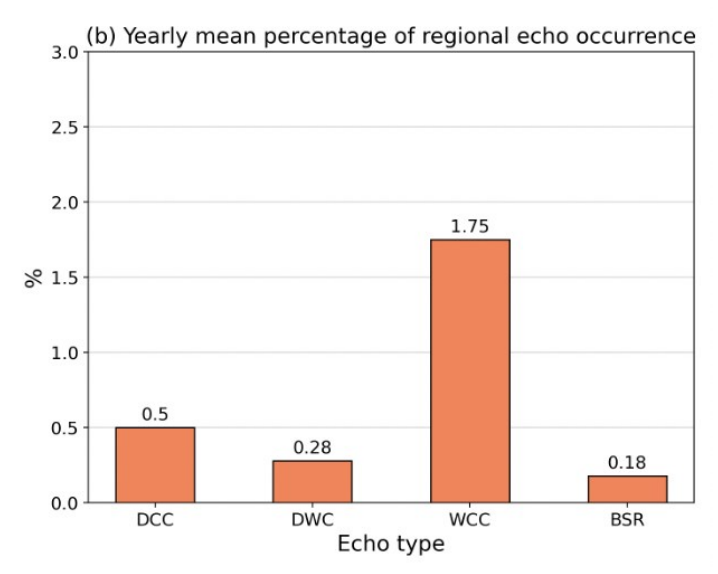


Figure 3: The yearly mean percentage of total volumetric rainfall (left column) and DRA echoes (right column) associated with each strong convective-stratiform category. Values are calculated at a 1.0° horizontal resolution. The black box in each figure represents the bounds of the study region.





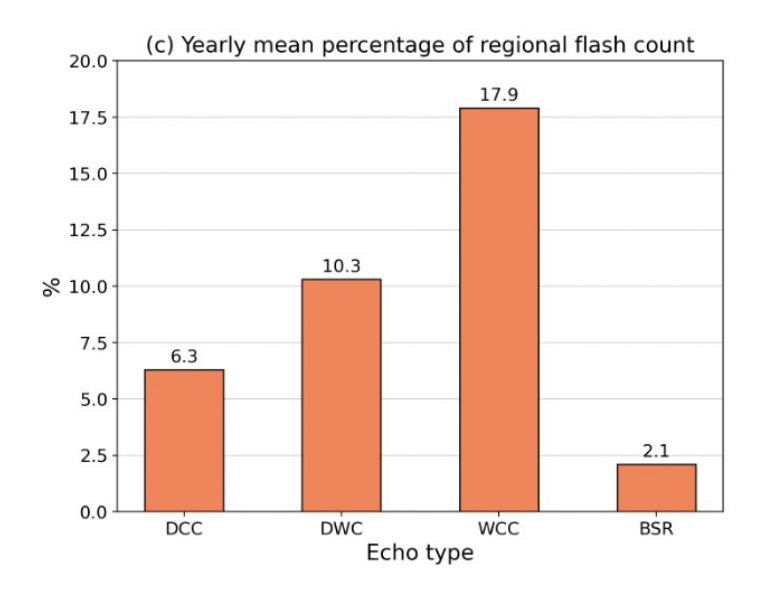


Figure 4: (a-c) The yearly mean percentage of regional rainfall, echo occurrence, and flash count associated with each strong convective-stratiform category.

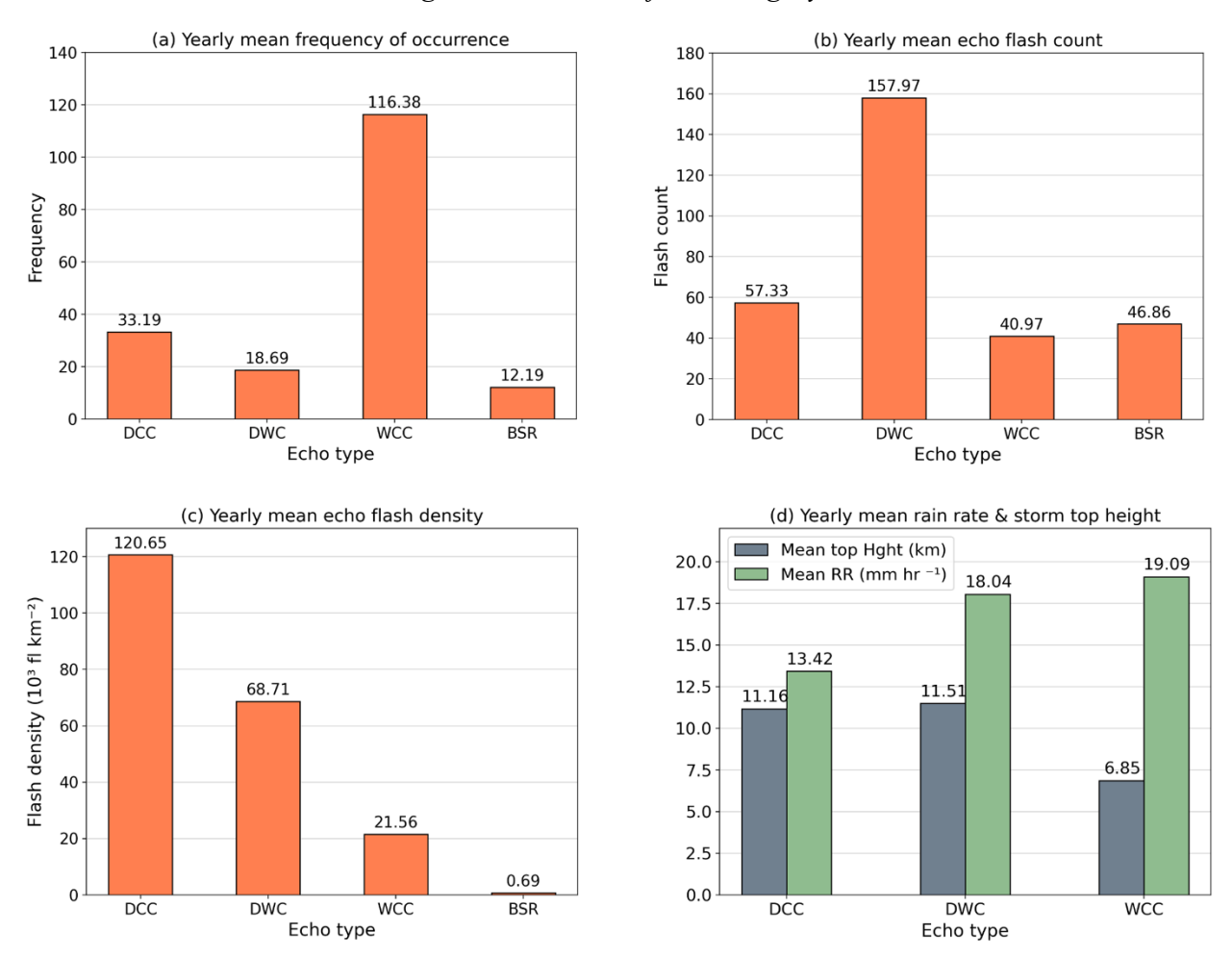


Figure 5: (a-c) Yearly mean frequency of echo occurrence (echoes yr^{-1}), echo lightning-flash count (fl echo⁻¹), and echo lightning-flash density (fl km^{-2}) associated with each strong convective-stratiform category. (d) yearly mean echo rain rate (mm hr^{-1}) (green) and echo top height (km) (grey) associated with each strong convective echo type.

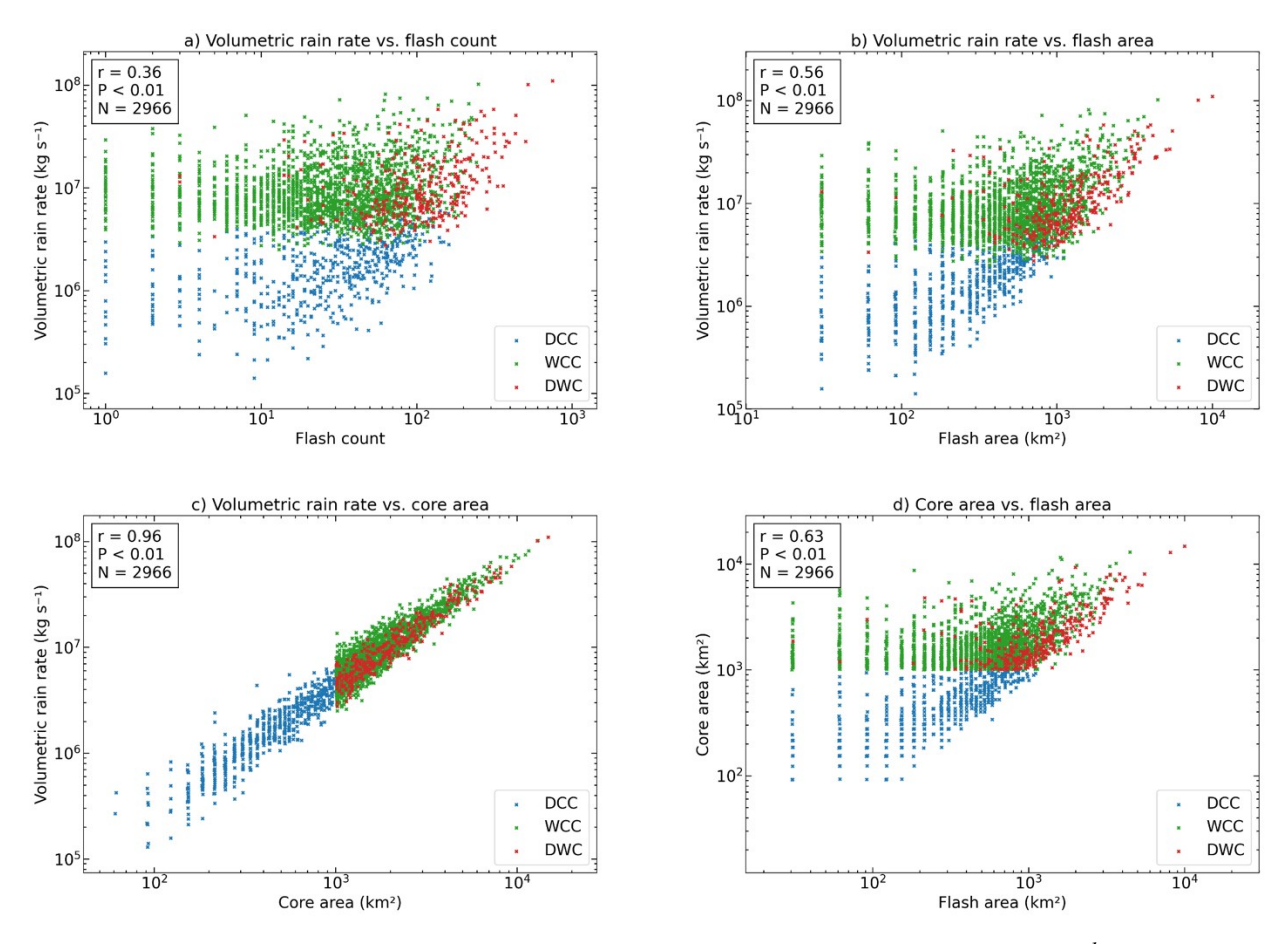


Figure 6: (a - d) Scatter plot of lightning-flash count vs. volumetric rain rate $(kg \ s^{-1})$, flash area (km^2) vs. volumetric rain rate, core area (km^2) vs. volumetric rain rate, and flash area vs. core area for echoes associated with DCCs (blue), WCCs (green), and DWCs (red).

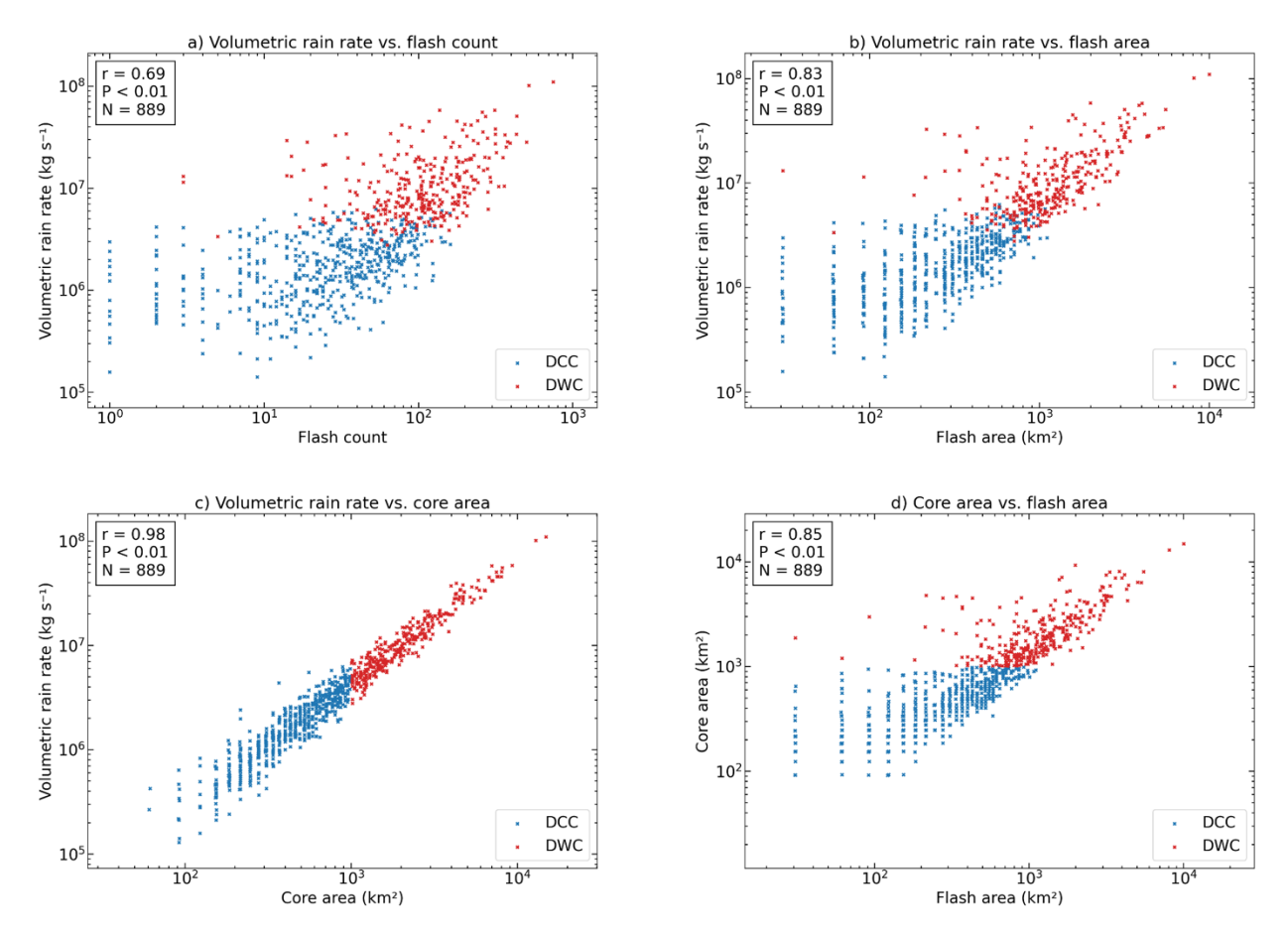


Figure 7: As in figure 6 but with WCCs removed from the data distribution.

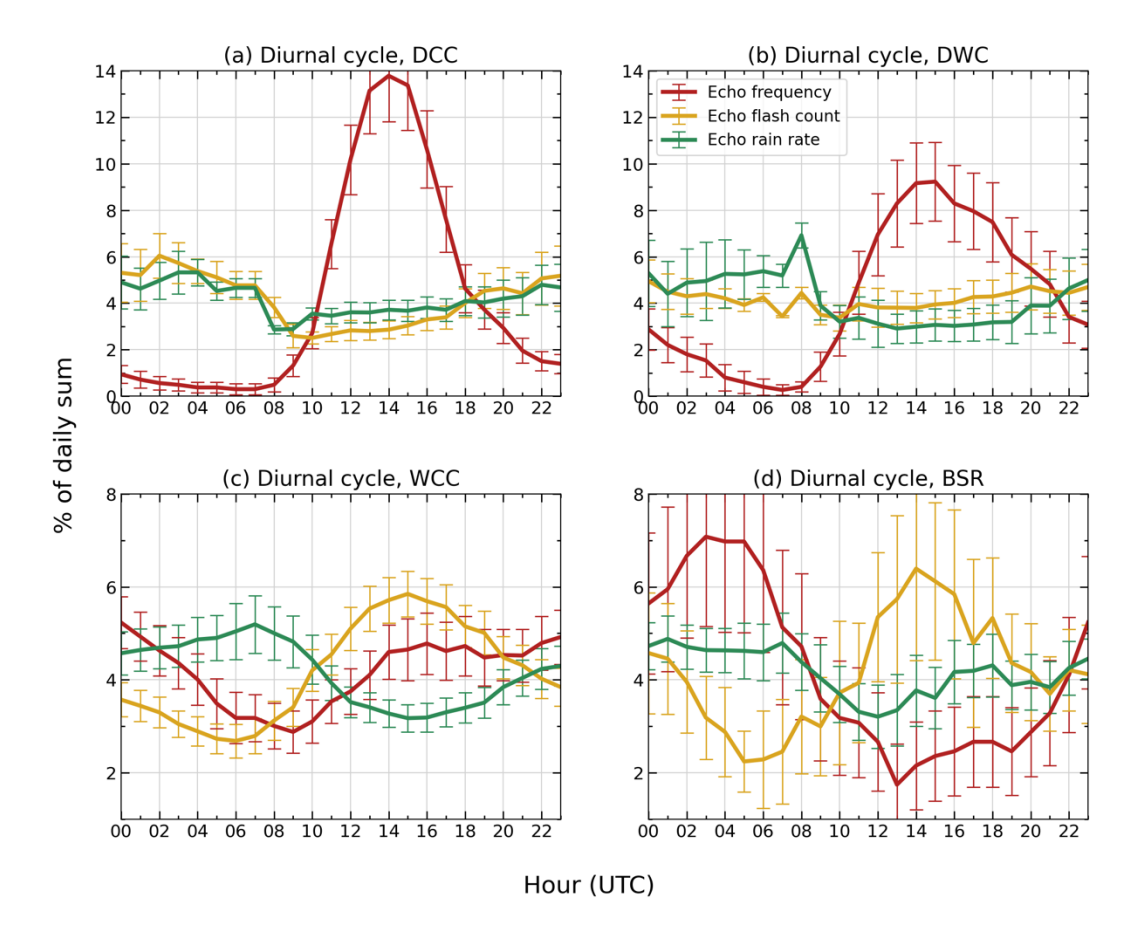


Figure 8: Diurnal cycles of the normalized yearly mean echo frequency of occurrence (red), mean echo flash count (fl echo⁻¹) (yellow), and mean echo volumetric rain (kg s⁻¹) (green) for (a) DCCs, (b) DWCs, (c) WCCs, and (d) BSRs. Error bars represent the standard error about the mean (SE). Values are expressed as percentages of their average daily sum.

References

- Adler, R.F., Negri, A.J., 1988. A Satellite Infrared Technique to Estimate Tropical Convective and Stratiform Rainfall. J. Appl. Meteorol. https://doi.org/10.1175/1520-0450(1988)027<0030:asitte>2.0.co;2
- Albrecht, R.I., Goodman, S.J., Peterson, W.A., Buechler, D.E., Bruning, E.C., Blakeslee, R.J., Christian, H.J., 2011. The 13 years of TRMM Lightning Imaging Sensor: From individual flash characteristics to decadal tendencies. XIV Int. Conf. Atmos. Electr. 8–12.
- Alsdorf, D., Beighley, E., Laraque, A., Lee, H., Tshimanga, R., O'Loughlin, F., Mahé, G., Dinga, B., Moukandi, G., Spencer, R.G.M., 2016. Opportunities for hydrologic research in the Congo Basin. Rev. Geophys. 54, 378–409. https://doi.org/10.1002/2016RG000517
- Arkin, P.A., 1979. The Relationship between Fractional Coverage of High Cloud and Rainfall Accumulations during GATE over the B-scale Array. Mon. Weather Rev. 107, 1382–1387.
- Arkin, P.A., Meisner, B.N., 1987. The Relationship between Large-Scale Convective Rainfall and Cold Cloud over the Western Hemisphere during 1982–84. Mon. Weather Rev. 115, 51–74.
- Arkin, P.A., Pingping Xie, 1994. The Global Precipitation Climatology Project: first algorithm intercomparison project. Bull. Am. Meteorol. Soc. 75, 401–419. https://doi.org/10.1175/1520-0477(1994)075<0401:TGPCPF>2.0.CO;2
- Atlas, D., Rosenfield, D., Short, D.A., 1990. The Estimation of Convective Rainfall by Area Integrals 1. The Theoretical and Empirical Basis. J. Geophys. Res. 95, 2153–2160.
- Ba, M.B., Gruber, A., 2001. GOES Multispectral Rainfall Algorithm (GMSRA). J. Appl. Meteorol. 40, 1500–1514. https://doi.org/10.1175/1520-0450(2001)040<1500:GMRAG>2.0.CO;2
- Bandholnopparat, K., Sato, M., Adachi, T., Ushio, T., Takahashi, Y., 2020. Estimation of the IC to CG Ratio Using JEM-GLIMS and Ground-Based Lightning Network Data. J. Geophys. Res. Atmos. 125, 0–3. https://doi.org/10.1029/2019JD032195
- Blakeslee, R.J., 2021. Lightning Imaging Sensor (LIS) on TRMM Science Data. Dataset available online from the NASA Global Hydrometeorology Resource Center DAAC, Huntsville, Alabama, U.S.A. DOI: http://dx.doi.org/10.5067/LIS/LIS/DATA201
- Bruning, E.C., Macgorman, D.R., 2013. Theory and observations of controls on lightning flash size spectra. J. Atmos. Sci. 70, 4012–4029. https://doi.org/10.1175/JAS-D-12-0289.1
- Carey, L.D., Murphy, M.J., McCormick, T.L., Demetriades, N.W.S., 2005. Lightning location relative to storm structure in a leading-line, trailing-stratiform mesoscale convective system. J. Geophys. Res. D Atmos. 110, 1–23. https://doi.org/10.1029/2003JD004371
- Cecil, D.J., Buechler, D.E., Blakeslee, R.J., 2014. Gridded lightning climatology from TRMM-LIS and OTD: Dataset description. Atmos. Res. 135–136, 404–414. https://doi.org/10.1016/j.atmosres.2012.06.028
- Cecil, D.J., Buechler, D.E., Blakeslee, R.J., 2015. TRMM LIS climatology of thunderstorm occurrence and conditional lightning flash rates. J. Clim. 28, 6536–6547.

- https://doi.org/10.1175/JCLI-D-15-0124.1
- Chaudhuri, S., Middey, A., 2014. Comparison of tropical and midlatitude thunderstorm characteristics anchored in thermodynamic and dynamic aspects. Asia-Pacific J. Atmos. Sci. 50, 179–189. https://doi.org/10.1007/s13143-014-0006-9
- Deierling, W., Petersen, W.A., 2008. Total lightning activity as an indicator of updraft characteristics. J. Geophys. Res. Atmos. 113. https://doi.org/10.1029/2007JD009598
- Ebert, E.E., Manton, M.J., 1998. Performance of satellite rainfall estimation algorithms during TOGA COARE. J. Atmos. Sci. 55, 1537–1557. https://doi.org/10.1175/1520-0469(1998)055<1537:POSREA>2.0.CO;2
- Fovell, R.G., 2002. Upstream influence of numerically simulated squall-line storms. Q. J. R. Meteorol. Soc. 128, 893–912. https://doi.org/10.1256/0035900021643737
- Gijben, M., 2012. The lightning climatology of South Africa. S. Afr. J. Sci. 108, 1–10. https://doi.org/10.4102/sajs.v108i3/4.740
- Gijben, M., de Coning, E., 2017. Using satellite and lightning data to track rapidly developing thunderstorms in data sparse regions. Atmosphere (Basel). 8. https://doi.org/10.3390/atmos8040067
- Grifith, C.G., Woodley, W.L., Grube, P.G., 1978. Rain Estimation from Geosynchronous Satellite Imagery Visible and Infrared Studies. Am. Meteorol. Soc. 106, 1153–1171.
- Holmlund, K., Grandell, J., Schmetz, J., Stuhlmann, R., Bojkov, B., Munro, R., Lekouara, M.,
 Coppens, D., Viticchie, B., August, T., Theodore, B., Watts, P., Dobber, M., Fowler, G.,
 Bojinski, S., Schmid, A., Salonen, K., Tjemkes, S., Aminou, D., & Blythe, P. (2021).
 Meteosat Third Generation (MTG): Continuation and Innovation of Observations from
 Geostationary Orbit, Bulletin of the American Meteorological Society, 102(5), E990-E1015.
- Hong, Y., Chen, S., Xue, X., Hodges, G., 2012. Global precipitation estimation and applications. In N. Chang & Y. Hong (Eds.), Multiscale hydrologic remote sensing: Perspectives and applications (pp. 371–386). Boca Raton, FL: CRC Press.
- Houze, R. A., Jr., 2004. Mesoscale convective systems. Rev. Geophys. 42. https://doi.org/10.1029/2004RG000150
- Houze, R.A., Jr., Wilton, D.C., Smull, B.F., 2007. Monsoon convection in the Himalayan region as seen by the TRMM precipitation radar. Q. J. R. Meteorol. Soc. 133, 1389–1411. https://doi.org/10.1002/qj.106
- Houze, R. A., Jr., K. L. Rasmussen, M. D. Zuluaga, and S. R. Brodzik, 2015. The variable nature of convection in the tropics and subtropics: A legacy of 16 years of the Tropical Rainfall Measuring Mission satellite. Rev. Geophys. 53. https://doi.org/10.1002/2015RG000488
- Jackson, B., Nicholson, S. E., & Klotter, D., 2009. Mesoscale Convective Systems over Western Equatorial Africa and Their Relationship to Large-Scale Circulation, Monthly Weather Review, 137(4), 1272-1294.
- Jiang, Y., Zhou L., Tucker, C.J., Raghavendra, A., Hua, W., Liu, Y., and Joiner, J., 2019.

- Widespread increase of boreal summer dry season length over the Congo rainforest. Nature Climate Change, 9, 617–622.
- Kidd, C., Kniveton, D.R., Todd, M.C., Bellerby, T.J., 2003. Satellite rainfall estimation using combined passive microwave and infrared algorithms. J. Hydrometeorol. 4, 1088–1104. https://doi.org/10.1175/1525-7541(2003)004<1088:SREUCP>2.0.CO;2
- Kidd, C., Levizzani, V., 2011. Status of satellite precipitation retrievals. Hydrol. Earth Syst. Sci. 15, 1109–1116. https://doi.org/10.5194/hess-15-1109-2011
- Kuhlman, K.M., MacGorman, D.R., Biggerstaff, M.I., Krehbiel, P.R., 2009. Lightning initiation in the anvils of two supercell storms. Geophys. Res. Lett. 36, 1–5. https://doi.org/10.1029/2008GL036650
- Kuligowski, R.J., 2002. A self-calibrating real-time GOES rainfall algorithm for short-term rainfall estimates. J. Hydrometeorol. 3, 112–130. https://doi.org/10.1175/1525-7541(2002)003<0112:ASCRTG>2.0.CO;2
- Laing, A.G., Carbone, R.E., Levizzani, V., 2011. Cycles and propagation of deep convection over equatorial Africa. Mon. Weather Rev. 139, 2832–2853. https://doi.org/10.1175/2011MWR3500.1
- Nag, A., Murphy, M.J., Schulz, W., Cummins, K.L., 2015. Lightning locating systems: Insights on characteristics and validation techniques. Earth and Space Sciencehttps://doi.org/10.1002/2014EA000051
- Negri, A.J., Adler, R.F., 1981. Relationship of satellite-based thunderstorm intensity to radarestimated rainfall. J. Appl. Meteor., 20, 288–300. https://doi.org/10.1175/1520-0450(1981)020<0288:ROSBTI>2.0.CO;2
- Negri, A.J., Bell, T.L., Xu, L., 2002. Sampling of the diurnal cycle of precipitation using TRMM. J. Atmos. Ocean. Technol. 19, 1333–1344. https://doi.org/10.1175/1520-0426(2002)019<1333:SOTDCO>2.0.CO;2
- Petersen, W.A., Christian, H.J., Rutledge, S.A., 2005. TRMM observations of the global relationship between ice water content and lightning. Geophys. Res. Lett. 32, 1–4. https://doi.org/10.1029/2005GL023236
- Price, C.G., 2013. Lightning Applications in Weather and Climate Research. Surv. Geophys. 34, 755–767. https://doi.org/10.1007/s10712-012-9218-7
- Raghavendra, A. 2020. Factors Influencing Rainfall over the Congo. Ph.D. dissertation, Department of Atmospheric and Environmental Sciences, University at Albany, 161 pp.
- Rasmussen, K.L., Houze, R.A., 2011. Orogenic convection in subtropical South America as seen by the TRMM satellite. Mon. Weather Rev. 139, 2399–2420. https://doi.org/10.1175/MWR-D-10-05006.1
- Schultz, E.V., C.J. Schultz, L.D. Carey, D.J. Cecil, and M. Bateman, 2016: Automated storm tracking and the lightning jump algorithm using GOES-R Geostationary Lightning Mapper (GLM) proxy data. J. Operational Meteor., 4 (7), 92–107, doi:

- http://dx.doi.org/10.15191/nwajom.2016.0407.
- Sorooshian, S., Hsu, K.L., Gao, X., Gupta, H. V., Imam, B., Braithwaite, D., 2000. Evaluation of PERSIANN system satellite-based estimates of tropical rainfall. Bull. Am. Meteorol. Soc. 81, 2035–2046. https://doi.org/10.1175/1520-0477(2000)081<2035:EOPSSE>2.3.CO;2
- Soula, S., Kasereka, J.K., Georgis, J.F., Barthe, C., 2016. Lightning climatology in the Congo Basin. Atmos. Res. 178–179, 304–319. https://doi.org/10.1016/j.atmosres.2016.04.006
- Thomas, R.J., Krehbiel, P.R., Rison, W., Hamlin, T., Boccippio, D.J., Goodman, S.J., Christian, H.J., 2000. Comparison of ground-based 3-dimensional lightning mapping observations with satellite-based LIS observations in Oklahoma, Geophys. Res. Lett., 27(12), 1703–1706.
- Todd, M.C., Kidd, C., Kniveton, D., Bellerby, T.J., 2001. A combined satellite infrared and passive microwave technique for estimation of small-scale rainfall. J. Atmos. Ocean. Technol. 18, 742–755. https://doi.org/10.1175/1520-0469(2001)058<0742:ACSIAP>2.0.CO;2
- Toracinta, E.R., Cecil, D.J., Zipser, E.J., Nesbitt, S.W., 2002. Radar, passive microwave, and lightning characteristics of precipitating systems in the tropics. Mon. Weather Rev. 130, 802–824. https://doi.org/10.1175/1520-0493(2002)130<0802:RPMALC>2.0.CO;2
- Ushio, T., Heckman, S., Driscoll, K., Boccippio, D., Christian, H., Kawasaki, Z., 2002. Crosssensor comparison of the lightning imaging sensor (LIS), Int. Remote Sens. J., 23(13), 2703–2712.
- Vicente, G.A., Scofield, R.A., Menzel, W.P., 1998. The Operational GOES Infrared Rainfall Estimation Technique. Bull. Am. Meteorol. Soc. 79, 1883–1893. https://doi.org/10.1175/1520-0477(1998)079<1883:togire>2.0.co;2
- Weiss, S.A., Macgorman, D.R., Calhoun, K.M., 2012. Lightning in the anvils of supercell thunderstorms. Mon. Weather Rev. 140, 2064–2079. https://doi.org/10.1175/MWR-D-11-00312.1
- Williams, E., Rosenfeld, D., Madden, N., Gerlach, J., Gears, N., Atkinson, L., Dunnemann, N., Frostrom, G., Antonio, M., Biazon, B., Camargo, R., Franca, H., Gomes, A., Lima, M., Machado, R., Manhaes, S., Nachtigall, L., Piva, H., Quintiliano, W., Machado, L., Artaxo, P., Roberts, G., Renno, N., Blakeslee, R., Bailey, J., Boccippio, D., Betts, A., Wolff, D., Roy, B., Halverson, J., Rickenbach, T., Fuentes, J., Avelino, E., 2002. Contrasting convective regimes over the Amazon: Implications for cloud electrification. J. Geophys. Res. Atmos. 107, 1–19. https://doi.org/10.1029/2001JD000380
- Xu, W., Adler, R.F., Wang, N.Y., 2013. Improving geostationary satellite rainfall estimates using lightning observations: Underlying lightning-rainfall-cloud relationships. J. Appl. Meteorol. Climatol. 52, 213–229. https://doi.org/10.1175/JAMC-D-12-040.1
- Yoshida, S., Morimoto, T., Ushio, T., Kawasaki, Z.I., 2009. A fifth-power relationship for lightning activity from Tropical Rainfall Measuring Mission satellite observations. J. Geophys. Res. Atmos. 114, 1–10. https://doi.org/10.1029/2008JD010370
- Yuan, T., Remer, L.A., Pickering, K.E., Yu, H., 2011. Observational evidence of aerosol enhancement of lightning activity and convective invigoration. Geophys. Res. Lett. 38, 1–5.

- https://doi.org/10.1029/2010GL046052
- Zhou, L., Tian, Y., Myneni, R.B., Ciais, P., Saatchi, S., Liu, Y.Y., Piao, S., Chen, H., Vermote, E.F., Song, C., Hwang, T., 2014. Widespread decline of Congo rainforest greenness in the past decade. Nature 508, 86–90. https://doi.org/10.1038/nature13265
- Zipser, E.J., 1994. Deep Cumulonimbus Cloud Systems in the Tropics with and without Lightning. Bull. Am. Meteorol. Soc. 122, 1837–1851.
- Zuluaga, M.D., Houze, R.A., 2015. Extreme convection of the near-equatorial Americas, Africa, and adjoining oceans as seen by TRMM. Mon. Weather Rev. 143, 298–316. https://doi.org/10.1175/MWR-D-14-00109.1
- Zuluaga, M.D., Houze, R.A., 2013. Evolution of the population of precipitating convective systems over the equatorial indian ocean in active phases of the Madden-Julian oscillation. J. Atmos. Sci. 70, 2713–2725. https://doi.org/10.1175/JAS-D-12-0311.1